Evidence of Ba-substitution induced spin-canting in the magnetic Weyl semimetal EuCd₂As₂

L. D. Sanjeewa,[1,*] J. Xing,[1,*] K. M. Taddei [2,*,†] D. Parker,[1] R. Custelcean,[3] C. dela Cruz,[2] and A. S. Sefat[1]

[1]*Materials Science and Technology Division, Oak Ridge National Laboratory, Oak Ridge, Tennessee 37831, USA*
[2]*Neutron Scattering Division, Oak Ridge National Laboratory, Oak Ridge, Tennessee 37831, USA*
[3]*Chemical Sciences Division, Oak Ridge National Laboratory, Oak Ridge, Tennessee 37831, USA*

Recently EuCd₂As₂ was predicted to be a magnetic Weyl semimetal with a lone pair of Weyl nodes generated by A-type antiferromagnetism and protected by a rotational symmetry. However, it was soon discovered that the actual magnetic structure broke the rotational symmetry and internal pressure was later suggested as a route to stabilize the desired magnetic state. In this work we test this prediction by synthesizing a series of Eu$_{1-x}$Ba$_x$Cd₂As₂ single crystals and studying their structural, magnetic, and transport properties via both experimental techniques and first-principles calculations. We find that small concentrations of Ba ($\sim$3%–10%) lead to a small out-of-plane canting of the Eu moment. However, for higher concentrations this effect is suppressed and a nearly in-plane model is recovered. Studying the transport properties we find that all compositions show evidence of an anomalous Hall effect dominated by the intrinsic mechanism as well as large negative magnetoresistances in the longitudinal channel. A nonmonotonic evolution of the transport properties is seen across the series which correlates to the proposed canting suggesting canting may enhance the topological effects. Careful density functional theory calculations using an all-electron approach revise prior predictions finding a purely ferromagnetic ground state with in-plane moments for both the EuCd₂As₂ and Eu$_{0.5}$Ba$_{0.5}$Cd₂As₂ compounds, corroborating our experimental findings. This work suggests that Ba substitution can tune the magnetic properties in unexpected ways which correlate to changes in measures of topological properties, encouraging future work to locate the ideal Ba concentration for Eu moment canting.

I. INTRODUCTION

Topological materials have garnered significant interest in the condensed matter community for their potential to unlock theoretically proposed computing paradigms via the realization of physics long constrained to the context of high-energy physics [1]. This broad novelty arises as topological materials eschew Landau classification and instead host electronic states engendered by topological invariants rather than broken symmetries giving rise to novel quasiparticles such as Dirac, Weyl, and Majorana fermions or even exotic long-range entangled states [1–3].

Of the former group of symmetry-protected topological sates, Weyl semimetals (WSMs) have received significant interest due to their potential applications in quantum devices ranging from photovoltaics to valleytronics to quantum computing [4–9]. However, while WSMs have great promise and numerous candidate materials have been discovered, there is some inherent difficulty in both finding unambiguous signatures of the Weyl physics and harnessing those properties for applications. One reason for this difficulty arises due to the presence of nontopological Fermi surfaces in many WSMs in addition to the Weyl points which lead to additional quasiparticles that can obscure the signatures of the Weyl

physics [10–12]. Additionally—and more detrimentally—many WSMs have multiple pairs of Weyl points which can thwart obvious signatures of the desired physics [11,13,14]. This second issue is partially inherent to the physics; for the majority of WSMs where inversion symmetry (IS) breaking is responsible for creating the Weyl points the minimal number of pairs of Weyl points is constrained to 4 and is often much higher such as 24 in the familiar TaAs compound [11,15]. The occurrence of numerous pairs of Weyl points leads to a corresponding complexity in their signatures which are then less easily identified.

However, there is a second class of WSMs in which time-reversal symmetry breaking gives rise to the Weyl physics [16,17]. In these magnetic Weyl semimetals (MWSMs) a minimum number of Weyl points—two—is possible [11]. If a material which realized this minimal case could be found it would allow for a more direct observation and potentially control of the Weyl physics [11]. Unfortunately, MWSMs have proven more difficult to find than the IS-breaking variety and of those discovered, many still manifest multiple pairs of Weyl nodes complicating their study [18,19].

Recently, EuCd₂As₂ (with centrosymmetric space group symmetry $P\overline{3}m1$) was predicted to be a MWSM with the minimal number of Weyl nodes [20]. Sorting through magnetic space group symmetries and their effects on the nodal Fermi surfaces, Hua *et al.* found that if a magnetic order was realized in EuCd₂As₂ which preserved the C_3 rotation axis via A-type antiferromagnetism (AFM) [i.e., c-polarized

Eu moments ferromagnetically (FM) coupled in-plane and AFM coupled out-of-plane] $EuCd_2As_2$ would go from a Dirac semimetal to a MWSM which realized only a single pair of Weyl nodes [20].

In the work that followed a more complex story emerged. Initial characterizations based on transport and magnetization measurements suggested the desired magnetic order with $T_N \sim 10$ K; however, followup reports using resonant x-ray scattering and density functional theory (DFT) calculations suggested the wanted FM and AFM intra- and interlayer correlations but with in-plane Eu moments [21–25]. Nonetheless, Hall effect (HE) measurements suggested a significant and gate-controllable anomalous Hall effect (AHE) and studies using applied magnetic fields showed that the c-polarized state could be achieved by applying a modest (~ 1.5 T) field along the c axis leading to sustained interest in $EuCd_2As_2$ [22,24,26].

Yet more recently, a careful study using muon spin rotation to probe the magnetic fluctuations suggested a novel behavior above T_N where intralayer magnetic interactions stabilized long-lived fluctuations of the c-polarized state which could generate the desired Weyl physics (identified via angle-resolved photoemission spectroscopy) [27]. Furthermore, additional DFT work proposed that weakening the interlayer Eu coupling via internal pressure though Ba substitution could stabilize the c-polarized FM state [28]. In their calculations Wang *et al.* suggest a Ba concentration of 50% (if assumed to separate into ordered Ba-only and Eu-only layers) could dilate the c axis enough to achieve the needed reduced interlayer coupling. Concurrently, a new synthesis study suggested another route to FM via the introduction of Eu vacancies [29]. In this work it was suggested that the in-plane AFM could be tuned to FM with a T_c of ~ 30 K via a small Eu deficiency (between 1% and 4%) thus adding another avenue to potentially achieve the desired phase [29].

In this report, we contribute to this search by following up on Wang *et al.*'s prediction, growing a series of Ba-substituted $EuCd_2As_2$ ($Eu_{1-x}Ba_xCd_2As_2$ with $x \leqslant 0.4$). Using transport, magnetization, x-ray diffraction, and DFT we find that while the Ba substitution drives the expected c-axis dilation it has a quite different effect on the magnetism than initially predicted, leading to a small canting of the Eu moments out-of-plane but only for small $x \leqslant 0.3$ concentrations. Furthermore, transport measurements show that over the whole series the intrinsic contribution dominates the AHE and that the proposed canting seems to correlate to increased (and significant) negative magnetoresistance (nMR) in the longitudinal channels. Finally, revisiting the DFT calculations we find that the parent compound exhibits a small in-plane magnetic anisotropy and is predicted to have the in-plane FM (as found in our experiments) as its ground state, though not owing to Eu vacancies. Turning to $Eu_{0.5}Ba_{0.5}Cd_2As_2$ we find little evidence to motivate a layer-separated state and that for either this assumed state or a random occupancy state the substitution of Eu with Ba actually stabilizes AFM. Nonetheless, our results show that Ba substitution can tune the magnetic structure—though in a more complicated fashion than previously proposed—and that that tuning correlates to promising changes in measurements expected to chart the topological properties.
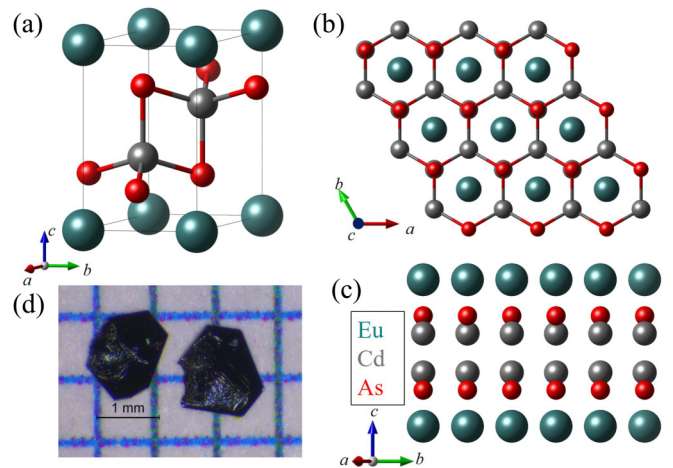

FIG. 1. Crystal lattice of $EuCd_2As_2$ viewed (a) parallel and (b) perpendicular to the Eu planes. (c) $EuCd_2As_2$ oriented to show the Eu-As-Cd-Cd-As-Eu stacking sequence. Eu, Cd, and As atoms are shown in teal, gray, and red, respectively. (d) shows representative shape and size of $Eu_{1-x}Ba_xCd_2As_2$ crystals.

II. METHODS

A. Synthesis

Single crystals of $EuCd_2As_2$ were grown using a flux method via a molten-salt media of KCl/NaCl (in an equimolar mixture). The reactants, Eu pieces, Cd pieces (Alfa Aesar, 99.99%), and As pieces (Alfa Aesar, 99.99%), were mixed with the salt flux in a He-purged dry box. In a typical reaction, a total of 1 g of Eu, Cd, and As were used in a stoichiometric ratio of $1:2:2$ with 10 g of total flux of KCl/NaCl. The reaction mixture was sealed in an evacuated fused-silica ampule and then heated to 497 °C at a rate of 20 °C/hr and held for one day, followed by another heating to 597 °C at a rate of 20 °C/hr and held for one day. After that, reactions were heated to 847 °C, 20 °C/hr, and held for 100 hr. As the final step, reactions were cooled to 500 °C at 1 °C/hr, and then furnace cooled to room temperature. Black shiny plate crystals were recovered by washing the product with deionized water using the vacuum filtration method. Single crystals were physically examined and selected under an optical microscope equipped with a polarizing light attachment (see Fig. 1). For $Eu_{1-x}Ba_xCd_2As_2$ the same method was employed with the appropriate stoichiometric amounts of Eu and Ba.

B. Characterization

For single-crystal x-ray diffraction (SXRD) studies, single crystals of $Eu_{1-x}Ba_xCd_2As_2$ were sonicated in acetone to remove any surface impurities. The SXRD was performed with a Bruker Quest D8 single-crystal x-ray diffractometer. The data were collected at room temperature utilizing Mo $K\alpha$ radiation, $\lambda = 0.71073$ Å. The crystal diffraction images were collected using ϕ and ω scans. The diffractometer was equipped with an Incoatec IμS source using the APEXIII software suite for data setup, collection, and processing [30]. All the structures were resolved using intrinsic phasing and full-matrix least-squares methods with refinement on F^2. All of the structure refinements were done using the SHELXTL

software suite [31]. All atoms were first refined with isotropic atomic displacement parameters which were later refined anisotropically.

Energy-dispersive spectroscopy analysis (EDS) was performed using a Hitachi S3400 scanning electron microscope equipped with an OXFORD EDX microprobe to confirm the elemental composition in all single-crystal samples. Powder x-ray diffraction (PXRD) data were collected using a PANalytical X'Pert Pro MPD diffractometer with Cu $K\alpha 1$ radiation ($\lambda = 1.5418$ Å) at room temperature. PXRD patterns of $EuCd_2As_2$ and $Eu_{1-x}Ba_xCd_2As_2$ were collected to identify the crystallographic plane of the flat surface of single crystals. Additionally, powder neutron diffraction patterns were collected for $Eu_{0.9}Ba_{0.1}Cd_2As_2$ on HB-2A of Oak Ridge National Laboratory's High Flux Isotope Reactor to attempt magnetic structure solution, as a further check of composition and to test the feasibility of neutron diffraction in a nonisotopic sample [32]. These data, however, proved difficult to analyze even qualitatively due to the large neutron absorption cross sections of both Eu and Cd (see the Supplemental Material (SM) [33]).

Temperature- and field-dependent magnetic measurements were carried out using a Quantum Design magnetic property measurement system (MPMS). The measurements were carried out on single-crystal specimens of $EuCd_2As_2$ and $Eu_{1-x}Ba_xCd_2As_2$ samples by orienting the crystals such that the Eu-Eu layers were aligned either parallel ($H \perp c$) or perpendicular ($H||c$) to the applied magnetic field. The temperature dependence of static susceptibility [$M/H(T)$] was measured over a temperature range of 2–50 K for the applied fields of 50 Oe. Isothermal magnetization measurements were performed at 2 K for fields up to 60 kOe.

Resistivity and Hall effect measurements were performed in a Quantum Design physical property measurement system (PPMS) using the standard four-point method. To ensure good results, the contact resistances were checked before each measurement and measurements were performed on multiple crystals of each composition. The crystal sizes were measured using a Leika microscope with a camera leading to an error of ~0.1 mm.

C. First-principles calculations

In an attempt to make sense of the magnetic and related behaviors observed in this system, we performed first-principles calculations using the all-electron plane-wave DFT code WIEN2k [34]. We began with the standard generalized gradient approximation (GGA) for structural refinements and moved to the GGA + U approach, with a U value of 5 eV applied to the Eu 4f orbitals, as used in previous work [28,35].

For the structure we used the lattice parameters of 4.45 and 7.35 Å for a and c, respectively (following the convention of previous work) [21,28]. We then relaxed the internal coordinates (with neither spin-orbit nor a U) within the unit cell with the one Eu spin-polarized (with a moment of essentially $7 \mu_B$), given that we are studying similar configurations for their magnetic characteristics. While we do not expect strong magnetoelastic coupling here given the generally localized nature of the magnetic Eu 4f orbitals (unlike recent work on
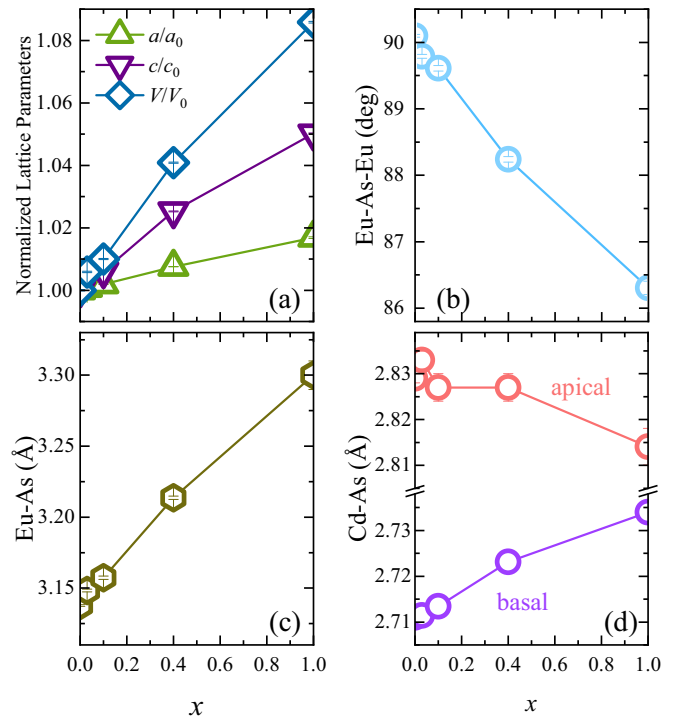

FIG. 2. Substitution dependence (in fractional Ba substitution) of the (a) normalized lattice parameters (normalized to the $EuCd_2As_2$ parent compound), (b) the Eu-As-Eu bond angle, (c) the Eu-As bond length, and (d) the basal and apical Cd-As bond lengths. Crystallographic parameters for the $BaCd_2As_2$ end member were taken from Ref. [41].

3d-based magnetic materials), it is best to take extra care with this computationally difficult system [36–38].

III. RESULTS AND DISCUSSION

A. Crystallographic properties

The nuclear crystal structure of $EuCd_2As_2$ is shown in Fig. 1. $EuCd_2As_2$ crystallizes in the centrosymmetric $P\bar{3}m1$ space group with Eu occupying the crystallographic $1a(0, 0, 0)$ Wyckoff position forming trigonal layers that alternate with layers of distorted edge-sharing $CdAs_4$ tetrahedra [where both Cd and As occupy the $2d(\frac{1}{3}, \frac{2}{3}, z)$ Wyckoff site]. The structure can be thought of as stacked triangular monoatomic layers of order Eu-As-Cd-Cd-As-Eu. In each layer the interatomic spacing is equivalent to the in-plane lattice parameter a with the interlayer distances varying due to the free z position of the Cd and As sites [Fig. 1(c)].

In Fig. 2 we plot the crystallographic parameters for $Eu_{1-x}Ba_xCd_2As_2$ with $x = 0$, 0.03, 0.1, and 0.4 extracted from Rietveld refinements performed using SXRD data collected at room temperature (numerical values are reported in the SM [33]). Starting with the parent compound, we find unit cell parameters similar to those reported previously with a and c of 4.4412 Å and 7.3255 Å, respectively [21,39]. For the internal parameters, the distorted $CdAs_4$ tetrahedra have one "apical" and 3 "basal" Cd-As bonds, the former of which is parallel to the c axis. Our refinements find the basal bonds to be 4% shorter at 2.7110(4) Å relative to

2.829(1) Å for the apical bond. Considering the Eu local environment, there is only one Eu-As bond at 3.1377 Å and one Eu-As-Eu bond angle, at 90.1(2)°—the latter of which is consistent with in-plane FM interactions considering the Goodenough-Kanamori rules for exchange interactions; these are, however, not always applicable to rare-earth superexchange [40].

Upon substituting Ba on the Eu site, we observe qualitatively the expected expansion of the lattice suggested by Wang *et al.* in Ref. [28] [see Fig. 2(a)]. The effect is anisotropic with the a axis expanding less than the c axis. Taking the 40% sample we find a ~0.5% expansion of the a axis and a ~2.5% expansion along c with an overall increase in the unit cell volume of ~4%. We note that this volume expansion is similar to the 4% expansion predicted by Wang *et al.* as needed to stabilize an out-of-plane magnetic order; however, our parent compound has a somewhat smaller unit cell than their DFT calculations and so our raw lattice parameters in the 40% are smaller than that predicted for the FM out-of-plane structure. Considering the lattice parameters separately our 40% sample's c axis is very near that predicted by Ref. [28] for $Eu_{0.5}Ba_{0.5}Cd_2As_2$. On the other hand, Wang *et al.*'s predicted a axis for the ideal $Eu_{0.5}Ba_{0.5}Cd_2As_2$ sample is actually larger than that reported for $BaCd_2As_2$ which we think unlikely in the absence of a structural transition upon Ba substitution [41].

Considering the bonding parameters, the Ba doping has little effect on the $CdAs_4$ tetrahedra, with the apical bond remaining essentially unchanged across the series and the three basal bonds expanding roughly commensurate with the change in the a axis [Fig. 2(d)]. On the other hand, the Eu-As bond continually dilates with doping and the Eu-As-Eu bond angle [Fig. 2(b)] is found to diverge from the nearly 90° found in the parent compound, monotonically decreasing to smaller angles with Ba substitution. Presumably, these latter changes may be the more significant as the Eu-As-Eu bond angle describes the superexchange pathway and so may affect the ground state magnetic structure.

As a check of our nominal compositions, we performed EDS analysis which showed the compositions to agree with the nominal stoichiometry to within the certainty of the technique (see SM [33]). As a second check, we also compared the obtained lattice parameters for all samples to those reported previously for $EuCd_2As_2$ and $BaCd_2As_2$ using Vegard's law [21,39,41,42]. Doing so results in calculated Ba concentrations in reasonable agreement with the nominal stoichiometry and EDS analysis. Finally, in the Rietveld refinements performed using our single-crystal XRD data, we allowed the Eu and Ba occupancies to refine. We found these refined occupancies to be in good agreement with our other measures. Therefore, we will use the nominal compositions throughout the text. As will become clear, it is important to note that we found no evidence of Eu vacancies in our parent compound in any of these tests. Furthermore, despite the predictions of Ref. [28], we saw no evidence of Eu-Ba ordering in our structure solution work; though we did not achieve the $Eu_{0.5}Ba_{0.5}Cd_2As_2$ composition exactly, as we will discuss later, we believe the Eu-Ba ordered phase to be unlikely to stabilize using the current synthesis techniques.
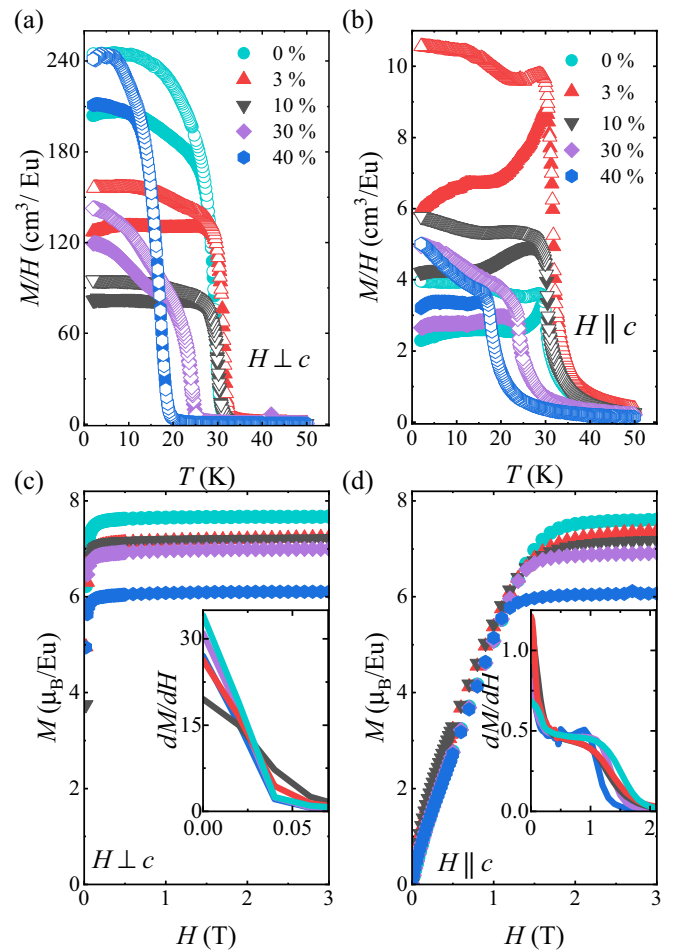

FIG. 3. Temperature-dependent magnetization of $Eu_{1-x}Ba_xCd_2As_2$ compositions for a probe field of 50 Oe applied (a) in the ab plane and (b) along the c axis. Closed circles are for measurements performed in zero field while open circles are for measurements performed in field-cooled warming. Magnetization field sweeps for field applied (c) in-plane and (d) along the c axis. Insets in (c) and (d) show the field derivative (dH/dM) for the two field orientations.

B. Magnetic properties

Having achieved some measure of lattice expansion we would like to study the magnetic properties to look for a change in the magnetic ground state. Shown in Figs. 3(a)–3(d) are the temperature- and field-dependent magnetization curves (normalized to Eu content) of all samples used in this study with the field applied both perpendicular and parallel to c and using both field-cooled on warming (FC) and zero-field-cooled (ZFC) procedures. Starting with the temperature dependence, we observe clear evidence of magnetic transitions in all samples, which we will label as a Curie temperature (T_c) rather than a Néel temperature (T_N) for reasons that will be clear later. For the parent compound, we see a T_c of ~29 K, with a large directional anisotropy where $H \perp c$ has a response two orders of magnitude larger at 2 K than the $H \| c$ direction. While this anisotropy is consistent with previous reports, the T_c we observe here is significantly higher

than what was found in the original reports of $T_N \sim 9$ K; we will discuss this discrepancy more later [21,22,24,27].

We next turn to the field-dependent magnetization measured at 2 K [Figs. 3(c) and 3(d)]. As seen, we observe behavior similar to previous reports, with a very rapid saturation for a field applied perpendicular to c (occurring at <0.3 T) and a somewhat slower response for a field applied along c (saturating at $\sim$1.5 T) [22,24]. For the saturated moment, we find $\sim$7.7(8) μ_B/Eu which is similar to that previously reported and within error of the expected value for an Eu^{2+} ion [24,29,43,44].

The significantly higher T_c we see in our $EuCd_2As_2$ compound is quite interesting. In a recent report (Ref. [29]), it was found that by varying synthesis conditions of $EuCd_2As_2$ the magnetic transition and, possibly, correlations could be tuned. In this work a sample with a similar T_c to ours is reported. There the authors suggest the change in the transition temperature is due to a slight ($\sim$1%–4%) Eu deficiency. Furthermore, they describe the resulting magnetic state as purely FM rather than the previously reported AFM.

While we think it likely that sample quality plays a role in the higher T_c, we are unable to confirm any such Eu vacancies in our sample via EDS or x-ray diffraction. Rather we find several observations to the contrary such as a larger unit cell volume in our sample, an increase in the per Eu saturated moment, and an effective moment in the paramagnetic state consistent with full occupancy [33,43]. None of these is consistent with the expectations of Eu vacancies characterized in Ref. [29]. As described, our synthesis procedure was quite deliberate and so we continue under the assumption of full Eu occupancy and attribute the change in T_c to different sample qualities. We leave it to future studies to uncover the cause of this intriguing divergence in the magnetic behavior of different $EuCd_2As_2$ samples.

Turning to the magnetization curve below the transition we observe different behavior than previously reported. For the in-plane magnetization we find behavior more typical of FM order where the magnetization increases with decreasing T until reaching a saturation point. In prior studies, a downturn was seen at lower temperatures which is not present here. For $H||c$ we find the previously reported temperature dependence with a sharp cusp followed by a drop and a soft shoulder with further decreasing temperature, the latter of which has been described as due to low-lying crystal field levels [24,29].

As a second characterization of the magnetism we look at the divergence of the FC and ZFC magnetizations [Figs. 3(a) and 3(b)]. In Ref. [24], the magnetic order along the two crystallographic directions was classified as either FM or AFM based on the FC/ZFC splitting—with a large splitting ostensibly resulting from alignment of the FM components of different magnetic domains. Rahn *et al.* reported a splitting of $\sim$15% for the in-plane magnetization and a splitting of <10% for $H||c$, and argued that this was consistent with FM order in-plane and AFM ordering between planes. In our measurements, we see splittings along both directions which are significantly larger (percent changes > 50%) than reported previously (measured with the same probe field) and of comparable size along the two directions. Considering the above arguments and those in Ref. [29], we suggest that the magnetic structure of the parent compound studied here is

likely purely FM with the moments pointing in-plane, thus indicating our labeling of our samples' transition temperatures as T_c.

We now consider the effects of Ba substitution on the magnetic properties. As shown in Figs. 3(c) and 3(d) Ba substitution leaves the magnetization field sweeps nearly unchanged qualitatively with similar saturation fields found for all measured compositions. However, a notable decrease in the saturated moment per Eu is seen with a decrease from 7.7(8) μ_B to 6.1(6) μ_B from the parent compound to 40% Ba (we again note that the reported magnetization is corrected for each composition's Eu content). Such a change in the per Eu moment is unexpected as Ba^{2+} and Eu^{2+} contribute the same number of electrons. Therefore, ignoring structural changes for the moment, since the electron count per Eu does not change, neither should the resultant quantum numbers nor the magnitude of the moment. One might expect the overall formula unit magnetization to decrease with Ba substitution as the concentration of the magnetic Eu decreases; however, the plots shown here are normalized for the Eu content of each composition and so suggest an actual reduction in the per Eu moment.

One potential cause is the lattice (and related Eu-As bond-length) dilation caused by the substitution of the larger Ba^{2+} ion on the Eu site. This in turn should alter the single-ion physics (such as the crystal field levels) and so may change the local moment [45]. However, changes in the local moment due to crystal field levels are usually larger discrete effects (such as going from a high-spin to a low-spin configuration) rather than the continuous decrease we report here. As another related possibility, the Ba sites may lead to a very local distortion which changes the ordered moment only of the surrounding Eu. This could lead to Eu neighboring Ba to have different moment sizes than the rest of the Eu sites with the reported magnetization being the average of the two. This could be consistent with changes to the local ion physics, with the continuous moment decrease arising as more of the Eu sites neighbor Ba. However, new measurements using local probes or techniques such as Mössbauer spectroscopy or total scattering would be necessary to corroborate this mechanism.

On the other hand, we can also speculate that such a decrease may be due to other more general effects such magnetic frustration. For a triangular magnetic lattice the introduction of nonmagnetic sites is well known as a potential route to magnetic frustration and even occasionally quantum magnetism [46–49]. With the substitution of nonmagnetic Ba onto the triangular magnetic Eu sublattice such effects seem likely and particularly interesting as they potentially indicate a route to novel physics. However, our current work does not allow for the discrimination between this, the local distortion, or another mechanism and so we leave this discussion to future work.

Looking next at the temperature dependence, we see that Ba substitution at first leaves T_c unchanged, with T_c in the parent compound and the 3% composition being identical within the temperature steps used here. However, as the substitution increases to 10% Ba we see a slight decrease in T_c to 27 K, a suppression which continues upon further doping dropping to 20 and 15 K for the 30% and 40% samples, respectively (we note that we used the criterion for determining T_c set in

Ref. [24], i.e., the peak of the ZFC $H||c$ curve). Considering that the $BaCd_2As_2$ end member is nonmagnetic, this suppression of T_c is not unexpected and is consistent with intuition that substituting a nonmagnetic ion on a magnetic site should disrupt the magnetic interactions [50,51].

More interestingly, if we look at the magnitude of the magnetization below the transition along the different directions we see different behavior than what might be expected from the field sweeps. As the Ba concentration increases, at first the magnetization along the c axis increases, with the largest increase of 160% seen in the 3% sample (for the ZFC measurements). Commensurately, for measurements along the in-plane direction we observe at first a steep decrease in the magnetization which drops by ~40% in the 3% sample. As the Ba concentration increases beyond 3% the response along c is seen to decrease, nearly returning to the parent compound's value by 40% while the in-plane response begins to increase until at 40% we again see it nearly return to the parent compound's value.

Considering the reduction in the in-plane magnetization and the seemingly coupled increase in the magnetization along the c axis we propose that the Ba substitution may drive a slight canting of the Eu moment out of the ab plane at intermediate concentrations (i.e., at 3%–10%). Upon further substitution the canting seems to be reduced returning (or nearly returning) to a purely in-plane structure by 40% (see the SM [33] for a qualitative phase diagram). As a second check of this, we take a closer look at the field sweeps, plotting their field derivative dM/dH in the insets of Figs. 3(c) and 3(d). Though the $M(H)$ curves look similar, the dM/dH curves reveal trends similar to that seen in the $M(T)$. Here both the 3% and 10% samples have a notably slower initial response to the applied field when it is applied in-plane, and a quicker response for $H||c$ than all other samples. This is consistent with the canting scenario, which, at least naively, should lead to a quicker c polarization saturation while requiring a larger field to saturate in-plane.

The mechanism for how this may happen is as of yet unknown, though previous experimental and theoretical work more generally on dilute nonmagnetic impurities in triangular lattice systems has shown planar to nonplanar transitions as a possibility [46,47,52,53]. In any case, the effects of nonmagnetic substitution are known to be complex with numerous perturbations such as local structural distortions due to size variance and disruption of magnetic interactions by nonmagnetic sites with all of this occurring on an already frustrated triangular lattice. Further studies are needed to understand the magnetic Hamiltonian which drives this behavior as well as diffraction (either with isotopic samples using neutrons or with resonant x-ray techniques) studies to confirm the proposed canting. However, if correct any such canting should have effects on the topological properties as the band structure is predicted to be sensitive to the moment direction [23,29].

C. Anomalous Hall effect and negative magnetoresistivity

With the magnetic effects of Ba substitution mapped we next look for evidence of changes in the topological physics
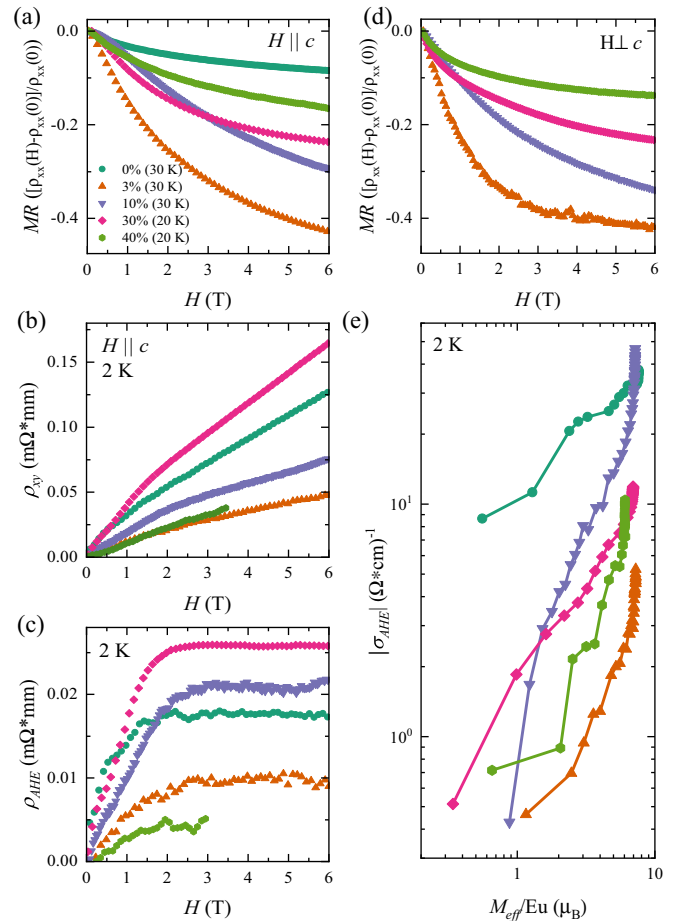

FIG. 4. (a) Magnetoresistance for $H||c$ for the listed compositions at temperatures just above T_c. (b) Hall resistivity (ρ_{xy}) for all samples collected at 2 K. (c) Anomalous Hall resistivity for all samples at 2 K achieved by subtracting the ordinary Hall effect contribution from the curves in panel (b). (d) Magnetoresistance of select samples for $H||E$ at the temperatures indicated in panel (a). (d) Absolute value of the anomalous Hall conductivities as a function of magnetization for all compositions at 2 K. The color scheme established in panel (a) for the compositions is continued throughout the figure.

via the transport properties (Fig. 4). To start we look at the transverse (Hall) resistivity ρ_{xy} [Fig. 4(b)] to look for the AHE. For a single-band conducting (or semiconducting) material an "ordinary Hall effect" (OHE) is expected which is proportional to the applied magnetic field H; for a FM, an additional AHE is expected [54]. The AHE itself can be derived from numerous phenomena only one of which (the intrinsic effect due to Berry curvature) is relevant to characterizing the topological properties [54]. Therefore, we will first separate the AHE and then perform further analysis to identify any intrinsic contribution.

To extract the AHE we utilize the familiar description of the Hall and AHE in a FM as $\rho_{xy} = R_0 H_z + R_s M_z$ with R_H, B, R_s, and M_z being the OHE coefficient, applied magnetic field perpendicular to the plane of measurement, AHE coefficient, and out-of-plane magnetization, respectively [55]. To isolate the AHE contribution we perform a linear fit to the

high-field region of Fig. 4(b), obtain R_0, and then subtract the $R_0 H_z$ term from ρ_{xy} to get just the anomalous term $\rho_{AHE} = \rho_{xy} - R_0 H_z$ [56]. We plot the resulting ρ_{AHE} in Fig. 4(c). As seen, the ρ_{AHE} contribution for all samples grows for low applied fields and saturates at about 1.5 T—similar to the applied fields at which the magnetization was seen to saturate in Fig. 3(d)—indicating the expected M dependence to this AHE term.

For ρ_{AHE} there are still three possible contributions: skew scattering and side jump which are due to disorder and impurity scattering and are dubbed extrinsic effects, and an intrinsic contribution which results from purely quantum effects related to the Berry curvature [54]. To start isolating the intrinsic contribution, we further separate ρ_{AHE} into two components based on its dependence on the longitudinal resistivity: $\rho_{AHE} = a\rho_{xx} + b\rho_{xx}^2$. In this form the linear term corresponds to skew scattering and the quadratic term corresponds to both the side-jump and intrinsic contributions [54,57–59]. To check for the skew-scattering contribution we use the temperature dependence of ρ_{xx} and the technique described in Ref. [57], where $\rho_{AHE}/(M\rho_{xx})$ is plotted against ρ_{xx} and the linear component is attributed to skew-scattering processes. If a linear regime can be found, it can be fitted and subtracted from ρ_{AHE}. Doing so here reveals only a small skew-scattering contribution to ρ_{xy} (see SM [33]) leaving either the side-jump or the intrinsic effect as dominant.

Due to their similar dependence on many of the available tuning parameters, the signatures of the side-jump and intrinsic mechanisms are difficult to separate. In Refs. [60] and [61] it is shown that for semiconducting FM plotting the AHE conductivity ($\sigma_{AHE} \sim \rho_{AHE}/\rho_{xx}^2$) as a function of the magnetization (M) allows for the identification of the intrinsic effect by looking for deviations from $\sigma_{AHE} \propto M$ with such deviations being a sign of strong spin-orbit coupling and therefore a dominant intrinsic term.

In Fig. 4(e) we plot $|\sigma_{AHE}(M)|$ for all samples on a log-log scale by combining the $M(H)$, $\rho_{AHE}(H)$, and $\rho_{xx}(H)$ data (as shown in Figs. 3(d), 4(a)–4(c), and the SM [33]). Here initially, $|\sigma_{AHE}|$ increases nearly linearly with M until the effective Eu moment is near its saturation value. As the magnetization increases further σ_{AHE} is seen to steeply increase nearly exponentially. In the theory work of Jungwirth *et al.* such an M dependence was found only for cases of very strong spin-orbit coupling (with a spin-orbit induced gap of ~ 0.1 eV) such as is consistent with the heavy Cd ion [61,62]. In such cases, their theory predicted a steep increase in σ_{AHE} at larger magnetization values similar to that seen here [61]. We note that we also determined $\sigma_{xy}(M)$ using the procedure used in Ref. [63] [where temperature-dependent $\sigma_{xy}(T)$ and $M(T)$ are used to plot $\sigma_{xy}(M)$ rather than $\sigma_{AHE}(H)$ and $M(H)$] and found similar nonlinearities; the results in Fig. 4(e) are not due to incomplete subtraction of the H dependence. As such we take the shape of our $|\sigma_{AHE}(M)|$ to indicate an AHE mainly derived from the intrinsic contribution. We refrain from commenting on the dependence of the AHE on Ba concentration due to the small differences and relative difficulty of the measurements, and instead leave the current analysis as showing that the large intrinsic AHE contribution persists across all compositions, and at least does not show

evidence of either a dramatic suppression or enhancement with Ba doping.

To help study the transport properties across samples, we turn to the longitudinal resistivity as expressed as a magnetoresistance [MR = $[\rho_{xx}(H) - \rho_{xx}(0)]/\rho_{xx}(0)$] which removes concerns of variations in absolute values which may be affected by systematic errors and derives of a single, large-signal measurement. Figure 4(a) shows the MR of all compositions just above T_c (where the MR was the largest though the trends hold for all temperatures measured) for the $H||c$ (i.e., $H \perp E$) configuration (we note that while we did not use a fine enough temperature grid to plot all samples for equal T/T_c, our conclusions are still valid considering the closeness of our temperatures to equal T/T_c and the temperature dependence of the MR; see SM [33]). All compositions show a significant nMR. While this is expected for a magnetic material, here we also observe a clear nonmonotonic trend in the magnitude of the nMR, with Ba concentration which is not expected [64]. The nMR increases from the parent compound to 3% and then decreases as the Ba concentration is increased further. Interestingly, though the nMR decreases beyond 3% the magnitude always remains larger than that of the parent compound. This behavior closely mirrors the nonmonotonic trend in the magnetization in the $H||c$ channel (Fig. 3).

In addition to the $H \perp E$ configuration, we also measured the MR of several samples with $H||E$ [Fig. 4(d)]. For a Weyl material, a nMR in this configuration is generally believed due to the chiral anomaly [65–69]. As for $H \perp E$ all measured samples show nMR of similar magnitude to the perpendicular direction. However, we caution that most treatments of the nMR due to the chiral anomaly are done for nonmagnetic materials. Here in the FM Eu$_{1-x}$Ba$_x$Cd$_2$As$_2$, it is possible that the nMR in this channel results from the same nontopological mechanism that contributes to the perpendicular direction: the alignment of the PM Eu moments. In this case, attributing this signal to the chiral anomaly becomes more suspect and so we resist drawing any significant conclusions from this observation.

.In general from these MR measurements we see some evidence of a novel effect on the transport properties of the Ba substitution. While the observation of the nMR might not be a smoking gun of Weyl physics in this material, the nonmonotonic behavior that mirrors the magnetization indicates that the doping is having a nontrivial effect. Though one might expect a decrease in the nMR with Ba substitution due to a reduction in the content of the magnetic Eu ion, the observation of a steep increase in the nMR after only a 3% substitution is not expected. Furthermore, though we do observe a reduction upon further substitution, the original value is never recovered, leaving the 40% with a larger nMR than the parent compound. Such results may derive of an additional contribution to the MR not seen in trivial FM and indicate some tuning of the magnetic and/or topological properties which are ostensibly responsible for the nMR in either channel. However, detailed theory work would be needed to extract the various possible contributions and so we leave the discussion here as only an interesting observation.

D. Density functional theory

Although a significant amount of theoretical work has been done on this system, both for pure $EuCd_2As_2$ and for Ba substitution, we revisit this work with an attempt to answer this operative question: What is the magnetic ground state of the $EuCd_2As_2$ system? While previous work (Ref. [28]) attempted to answer this question, it used a pseudopotential approach. Rare-earth magnetic properties are notoriously difficult to capture with such approaches, as may be gathered from recent work on potential rare-earth permanent magnet materials (e.g., Refs. [70] and [71]), and so we here revisit this question using a more accurate all-electron approach.

In the straight GGA we find that a FM configuration of the Eu, both within layers and between layers, is more stable than an AFM layer configuration (termed AFMA in the previous work of Ref. [28]) by some 3.7 meV per Eu. This is a rather large value and, although we have not calculated the Curie point, might suggest an ordering point significantly above that observed. With the application of a U of 5 eV and spin-orbit the FM state remains more stable by 0.4 meV per Eu, in contrast to the previous theoretical result where an AFM interlayer state was asserted. We believe the difference is due to the combination of our use of an all-electron approach, as well as the computational sensitivity of this system. For example, in these calculations a straight GGA calculation of a 4-layer state $Eu_2Ba_2Cd_8As_8$ with the Eu ferromagnetically coupled resulted in a clearly metastable configuration with one Eu showing the typical 7 μ_B spin moment and the other showing *no* moment. These concerns aside, this theoretical finding of an FM ground state is clearly supported by our experimental work so that for this study we regard the matter as resolved (see SM [33] for more discussion on the FM ground state).

We have also endeavored to calculate the magnetic anisotropy (MAE), to determine whether the substantial Eu moments prefer a uniaxial or planar orientation, which bears on the Weyl physics. In general, this is a difficult calculation, given that the approximate 1.5 T experimental anisotropy field and ~0.6 T saturation magnetization together imply an MAE of no more than 0.2 meV per Eu atom. While the calculations are of sufficient precision and accuracy to resolve this difference, rare-earth magnetic anisotropy, even within this accurate all-electron approach, remains a challenging task (please see Refs. [72,73] for examples of reasonably successful efforts in this area).

Within the computational approach outlined above, and exceedingly careful convergence checks involving, respectively, 5 000, 10 000, 20 000, 40 000 and as many as 75 000 k points, we find a very small, likely planar magnetic anisotropy of order 20 μeV/Eu, very near the accuracy limit of the calculations. Even at the finest k-point grid this result is not sufficiently converged to the usual standards of accuracy (10% or less variation). We can state with confidence, however, that the actual theoretical value is much smaller than the experimental value, and the use of a larger U of 8 eV does not resolve this discrepancy [74].

From a theoretical perspective, one would expect only a small magnetic anisotropy given than divalent Eu has a nearly exactly half-filled $4f$ shell, so that Hund's rules would nominally imply zero orbital moment. However, given the noncubic crystal field there is in the calculations a very small orbital moment of order 0.015 μ_B/Eu, which does lead to a finite though small anisotropy. This orbital moment and anisotropy are much smaller than commonly found in rare-earth magnetic materials and derive principally from the unique character of divalent, half-$4f$-shell-filled Eu [75].

We have also made investigations into the effects of Ba alloying on the magnetic character, given the previous suggestion of associated Weyl physics in a FM state induced via Ba alloying. For this, we have simulated a 50% concentration of Ba within two states—one in which the Ba and Eu reside in separate layers ("segregated FM case"), and one ("mixing FM case") in which they reside in the same layer. We have chosen lattice parameters by increasing them proportionally from our experimental values for the 40% Ba case, relative to the pure Eu case, and separately relaxed the internal coordinates within each configuration. We have also studied an interlayer "AFMA" state, in which the Eu and Ba layers alternate and there is an additional alternation of Eu moment orientation between Eu layers 2 c-axis lattice constants apart. For simplicity, these calculations were conducted within the straight GGA, without spin-orbit or a U; inclusion of these effects would likely only reduce the interlayer coupling, as in the previous results.

As in the previous results, we find from theory the "segregated FM" case to be the most energetically stable—some 68 meV per 10-atom cell below the "mixing FM" case and about 4 meV below the AFMA case [28]. Note that our XRD results find no evidence for the segregated FM case but rather find the "mixing FM" structure to be the magnetic ground state. We believe the reason for this discrepancy is the following: At typical synthesis conditions of 1000 K and above, there is a substantial entropic tendency for the divalent Eu and Ba atoms to mix on a layer (the "mixing FM" state), given that this is a lower-symmetry state than the "segregated FM" state. This entropic tendency is $-k_B T_{synth} \ln(2)$ per Eu/Ba atom, or about -120 meV per 10-atom unit cell, and generally more than compensates for the energetic stability of the "segregated FM" state. This suggests that careful low-temperature synthesis (ideally at temperatures below 600 K) may be necessary to stabilize a "segregated FM" state for 50% Ba alloying.

IV. CONCLUSIONS

Inspired by DFT predictions of a c-polarized FM state in $Eu_{0.5}Ba_{0.5}Cd_2As_2$, we performed XRD, magnetization, and transport measurements on a series of $Eu_{1-x}Ba_xCd_2As_2$ samples. Using a careful synthesis procedure we were able to grow high-quality single crystals of $Eu_{1-x}Ba_xCd_2As_2$ with $x \leqslant 0.4$. Our XRD work showed that Ba does indeed dilate the lattice, and that by $x = 0.4$ we achieve a c lattice previously predicted to stabilize the c-polarized FM state. However, magnetization measurements revealed that while Ba substitution does appear to cause out-of-plane canting of the Eu moments, the effect is small and occurs for much lower concentrations than predicted (i.e., 3%–10%). Additionally, we found that using our deliberate synthesis techniques, all compositions (including the parent compound) show purely FM order with T_c starting at ~30 K and being suppressed with increasing Ba concentration. Looking at the transport

properties, we found an AHE in all compositions that likely results from a dominant intrinsic contribution. Furthermore, measurements of the magnetoresistance revealed a large nMR in all samples and showed nonmonotonic behavior across the series that correlates to the magnetization with the 3% and 10% samples having the largest nMR.

More speculatively, we observe a suppression of the saturated moment with Ba substitution likely indicating frustration physics, and see behaviors in the MR in the $H||E$ channel which may hint at the chiral anomaly. Our work shows that Ba substitution has an ability to tune the magnetic and likely topological properties, encouraging follow-up scattering, DFT, and synthesis work to determine or confirm the canting, attempt to maximize it via a smaller concentration grid at low substitutions, follow the topological properties as a function of Ba concentration, and study how the numerous perturbations of Ba substitution may tune the magnetic Hamiltonian. This work could lead to a better understanding of how to stabilize the much sought after c-FM phase in $EuCd_2As_2$ and in doing so optimize conditions for the realization of Weyl physics in this rare magnetic Weyl semimetal.

[1] X.-G. Wen, Rev. Mod. Phys. **89**, 041004 (2017).

[2] A. Bansil, H. Lin, and T. Das, Rev. Mod. Phys. **88**, 021004 (2016).

[3] A. Burkov, Nat. Mater. **15**, 1145 (2016).

[4] G. B. Osterhoudt, L. K. Diebel, M. J. Gray, X. Yang, J. Stanco, X. Huang, B. Shen, N. Ni, P. J. Moll, Y. Ran *et al.*, Nat. Mater. **18**, 471 (2019).

[5] C.-K. Chan, P. A. Lee, K. S. Burch, J. H. Han, and Y. Ran, Phys. Rev. Lett. **116**, 026805 (2016).

[6] C.-K. Chan, N. H. Lindner, G. Refael, and P. A. Lee, Phys. Rev. B **95**, 041104(R) (2017).

[7] S. A. Parameswaran, T. Grover, D. A. Abanin, D. A. Pesin, and A. Vishwanath, Phys. Rev. X **4**, 031035 (2014).

[8] D. E. Kharzeev and Q. Li, arXiv:1903.07133.

[9] S. Jia, S.-Y. Xu, and M. Z. Hasan, Nat. Mater. **15**, 1140 (2016).

[10] G. B. Halász and L. Balents, Phys. Rev. B **85**, 035103 (2012).

[11] N. P. Armitage, E. J. Mele, and A. Vishwanath, Rev. Mod. Phys. **90**, 015001 (2018).

[12] B. Ramshaw, K. Modic, A. Shekhter, Y. Zhang, E.-A. Kim, P. Moll, M. Bachmann, M. Chan, J. Betts, F. Balakirev *et al.*, Nat. Commun. **9**, 1 (2018).

[13] S. Wang, B.-C. Lin, A.-Q. Wang, D.-P. Yu, and Z.-M. Liao, Adv. Phys.: X **2**, 518 (2017).

[14] B. Yan and C. Felser, Annu. Rev. Condens. Matter Phys. **8**, 337 (2017).

[15] H. Weng, C. Fang, Z. Fang, B. A. Bernevig, and X. Dai, Phys. Rev. X **5**, 011029 (2015).

[16] Z. Wang, X.-L. Qi, and S.-C. Zhang, New J. Phys. **12**, 065007 (2010).

[17] T. L. Hughes, E. Prodan, and B. A. Bernevig, Phys. Rev. B **83**, 245132 (2011).

[18] D. Liu, A. Liang, E. Liu, Q. Xu, Y. Li, C. Chen, D. Pei, W. Shi, S. Mo, P. Dudin *et al.*, Science **365**, 1282 (2019).

[19] G. Chang, B. Singh, S.-Y. Xu, G. Bian, S.-M. Huang, C.-H. Hsu, I. Belopolski, N. Alidoust, D. S. Sanchez, H. Zheng, H. Lu, X. Zhang, Y. Bian, T.-R. Chang, H.-T. Jeng, A. Bansil, H. Hsu, S. Jia, T. Neupert, H. Lin, and M. Z. Hasan, Phys. Rev. B **97**, 041104(R) (2018).

[20] G. Hua, S. Nie, Z. Song, R. Yu, G. Xu, and K. Yao, Phys. Rev. B **98**, 201116(R) (2018).

[21] I. Schellenberg, U. Pfannenschmidt, M. Eul, C. Schwickert, and R. Pöttgen, Z. Anorg. Allg. Chem. **637**, 1863 (2011).

[22] H. P. Wang, D. S. Wu, Y. G. Shi, and N. L. Wang, Phys. Rev. B **94**, 045112 (2016).

[23] J. Krishna, T. Nautiyal, and T. Maitra, Phys. Rev. B **98**, 125110 (2018).

[24] M. C. Rahn, J.-R. Soh, S. Francoual, L. S. I. Veiga, J. Strempfer, J. Mardegan, D. Y. Yan, Y. F. Guo, Y. G. Shi, and A. T. Boothroyd, Phys. Rev. B **97**, 214422 (2018).

[25] J.-R. Soh, F. de Juan, M. G. Vergniory, N. B. M. Schröter, M. C. Rahn, D. Y. Yan, J. Jiang, M. Bristow, P. A. Reiss, J. N. Blandy, Y. F. Guo, Y. G. Shi, T. K. Kim, A. McCollam, S. H. Simon, Y. Chen, A. I. Coldea, and A. T. Boothroyd, Phys. Rev. B **100**, 201102(R) (2019).

[26] C. Niu, N. Mao, X. Hu, B. Huang, and Y. Dai, Phys. Rev. B **99**, 235119 (2019).

[27] J.-Z. Ma, S. Nie, C. Yi, J. Jandke, T. Shang, M. Yao, M. Naamneh, L. Yan, Y. Sun, A. Chikina, V. Strocov, M. Medarde, M. Song, Y.-M. Xiong, G. Xu, W. Wulfhekel, J. Mesot, M. Reticcioli, C. Franchini, C. Mudry, M. Müller, Y. Shi, T. Qian, H. Ding, and M. Shi, Sci. Adv. **5**, eaaw4718 (2019).

[28] L.-L. Wang, N. H. Jo, B. Kuthanazhi, Y. Wu, R. J. McQueeney, A. Kaminski, and P. C. Canfield, Phys. Rev. B **99**, 245147 (2019).

[29] N. H. Jo, B. Kuthanazhi, Y. Wu, E. Timmons, T.-H. Kim, L. Zhou, L.-L. Wang, B. G. Ueland, A. Palasyuk, D. H. Ryan, R. J. McQueeney, K. Lee, B. Schrunk, A. A. Burkov, R. Prozorov, S. L. Bud'ko, A. Kaminski, and P. C. Canfield, Phys. Rev. B **101**, 140402(R) (2020).

[30] Bruker Advanced X-Ray Solutions, Madison, WI, USA.

[31] G. M. Sheldrick, Acta Crystallogr. Sect. A **64**, 112 (2008).

[32] S. Calder, K. An, R. Boehler, C. Dela Cruz, M. Frontzek, M. Guthrie, B. Haberl, A. Huq, S. A. Kimber, J. Liu *et al.*, Rev. Sci. Instrum. **89**, 092701 (2018).

[33] See Supplemental Material at http://link.aps.org/supplemental/10.1103/PhysRevB.102.104404 for details pertaining to sample synthesis, diffraction data collection, Rietveld refinements, and a more in depth discussion of the DFT results.

[34] P. Blaha, K. Schwarz, G. K. H. Madsen, D. Kvasnicka, J. Luitz, R. Laskowski, F. Tran, and L. D. Marks, *WIEN2k, An Augmented Plane Wave + Local Orbitals Program for Calculating Crystal Properties* (Karlheinz Schwarz, Technische Universität Wien, Austria, 2018).

[35] J. P. Perdew, K. Burke, and M. Ernzerhof, Phys. Rev. Lett. **77**, 3865 (1996).

[36] A. S. Sefat, L. Li, H. B. Cao, M. A. McGuire, B. Sales, R. Custelcean, and D. S. Parker, Sci. Rep. **6**, 1 (2016).

[37] G. Pokharel, A. F. May, D. S. Parker, S. Calder, G. Ehlers, A. Huq, S. A. J. Kimber, H. S. Arachchige, L. Poudel, M. A. McGuire, D. Mandrus, and A. D. Christianson, Phys. Rev. B **97**, 134117 (2018).

[38] K. Y. Chen, B. S. Wang, J.-Q. Yan, D. S. Parker, J.-S. Zhou, Y. Uwatoko, and J.-G. Cheng, Phys. Rev. Materials **3**, 094201 (2019).

[39] A. Artmann, A. Mewis, M. Roepke, and G. Michels, Z. Anorg. Allg. Chem. **622**, 679 (1996).

[40] W. Geertsma, Physica B (Amsterdam) **164**, 241 (1990).

[41] P. Klüfers and A. Mewis, Z. Kristallogr. **169**, 135 (1984).

[42] L. Vegard, Z. Phys. **5**, 17 (1921).

[43] J. Jensen and A. R. Mackintosh, *Rare Earth Magnetism* (Clarendon Press, Oxford, 1991).

[44] J.-Z. Ma, H. Wang, S.-M. Nie, C.-J. Yi, Y.-F. Xu, H. Li, J. Jandke, W. Wulfhekel, Y.-B. Huang, D. West, P. Richard, A. Chikina, V. Strocov, J. Mesot, H.-M. Weng, S.-B. Zhang, Y.-G. Shi, T. Qian, M. Shi, and H. Ding, Adv. Mater. **32**, 1907565 (2020).

[45] F. Jlaiel, M. Amami, P. Strobel, and A. Salah, Open Chemistry **9**, 953 (2011).

[46] A. I. Smirnov, T. A. Soldatov, O. A. Petrenko, A. Takata, T. Kida, M. Hagiwara, A. Y. Shapiro, and M. E. Zhitomirsky, Phys. Rev. Lett. **119**, 047204 (2017).

[47] V. S. Maryasin and M. E. Zhitomirsky, Phys. Rev. Lett. **111**, 247201 (2013).

[48] Y. Wang, Q. Guo, Y. Zou, W. Tong, Y. Liu, G. Gong, Y. Su, S. Yuan, and Z. Tian, Europhys. Lett. **124**, 27002 (2018).

[49] S. Dey, E. C. Andrade, and M. Vojta, Phys. Rev. B **101**, 020411(R) (2020).

[50] X. Yang, Y. Li, P. Zhang, H. Jiang, Y. Luo, Q. Chen, C. Feng, C. Cao, J. Dai, Q. Tao, G. Cao, and Z.-A. Xu, J. Appl. Phys. **114**, 223905 (2013).

[51] H. Kunioka, K. Kihou, H. Nishiate, A. Yamamoto, H. Usui, K. Kuroki, and C. Lee, Dalton Trans. **47**, 16205 (2018).

[52] T. Nakajima, S. Mitsuda, S. Kanetsuki, K. Tanaka, K. Fujii, N. Terada, M. Soda, M. Matsuura, and K. Hirota, Phys. Rev. B **77**, 052401 (2008).

[53] V. S. Maryasin and M. E. Zhitomirsky, J. Phys.: Conf. Ser. **592**, 012112 (2015).

[54] N. Nagaosa, J. Sinova, S. Onoda, A. H. MacDonald, and N. P. Ong, Rev. Mod. Phys. **82**, 1539 (2010).

[55] F. E. Maranzana, Phys. Rev. **160**, 421 (1967).

[56] B. Meng, H. Wu, Y. Qiu, C. Wang, Y. Liu, Z. Xia, S. Yuan, H. Chang, and Z. Tian, APL Mater. **7**, 051110 (2019).

[57] C. Zeng, Y. Yao, Q. Niu, and H. H. Weitering, Phys. Rev. Lett. **96**, 037204 (2006).

[58] J. Smit, Physica (Amsterdam) **24**, 39 (1958).

[59] L. Berger, Phys. Rev. B **2**, 4559 (1970).

[60] N. Manyala, Y. Sidis, J. F. DiTusa, G. Aeppli, D. P. Young, and Z. Fisk, Nat. Mater. **3**, 255 (2004).

[61] T. Jungwirth, Q. Niu, and A. H. MacDonald, Phys. Rev. Lett. **88**, 207208 (2002).

[62] F. L. Pedrotti and D. C. Reynolds, Phys. Rev. **127**, 1584 (1962).

[63] Z. Fang, N. Nagaosa, K. S. Takahashi, A. Asamitsu, R. Mathieu, T. Ogasawara, H. Yamada, M. Kawasaki, Y. Tokura, and K. Terakura, Science **302**, 92 (2003).

[64] W. A. Reed and E. Fawcett, Phys. Rev. **136**, A422 (1964).

[65] D. T. Son and B. Z. Spivak, Phys. Rev. B **88**, 104412 (2013).

[66] A. A. Burkov, Phys. Rev. B **91**, 245157 (2015).

[67] H. Ishizuka and N. Nagaosa, Phys. Rev. B **99**, 115205 (2019).

[68] C.-Z. Li, L.-X. Wang, H. Liu, J. Wang, Z.-M. Liao, and D.-P. Yu, Nat. Commun. **6**, 10137 (2015).

[69] Q. Li, D. Kharzeev, C. Zhang, Y. Huang, I. Pletikosić, A. Fedorov, R. Zhong, J. Schneeloch, G. Gu, and T. Valla, Nat. Phys. **12**, 550 (2016).

[70] W. Körner, G. Krugel, and C. Elsässer, Sci. Rep. **6**, 1 (2016).

[71] G. Krugel, W. Körner, D. F. Urban, O. Gutfleisch, and C. Elsässer, Metals **9**, 1096 (2019).

[72] T. Pandey and D. S. Parker, Phys. Rev. Appl. **13**, 034039 (2020).

[73] T. Pandey, M.-H. Du, and D. S. Parker, Phys. Rev. Appl. **9**, 034002 (2018).

[74] D. B. Ghosh, M. De, and S. K. De, Phys. Rev. B **70**, 115211 (2004).

[75] P. Larson, I. Mazin, and D. Papaconstantopoulos, Phys. Rev. B **67**, 214405 (2003).

[76] See http://energy.gov/downloads/doe-public-access-plan.